Available online at www.sciencedirect.com

ScienceDirect

Nuclear Physics A 982 (2019) 899–902

www.elsevier.com/locate/nuclphysa

XXVIIth International Conference on Ultrarelativistic Nucleus-Nucleus Collisions (Quark Matter 2018)

Recent results for STAR $\sqrt{s_{NN}}$ = 4.9 GeV Al+Au and $\sqrt{s_{NN}}$ = 4.5 GeV Au+Au Fixed-Target Collisions

Yang Wu for the STAR Collaboration[1]

Kent State University, Kent, Ohio 44242, USA

Abstract

We present recent results from Al(beam)+Au(target) collisions at $\sqrt{s_{NN}}$ = 4.9 GeV and Au+Au collisions at $\sqrt{s_{NN}}$ = 4.5 GeV from the STAR fixed-target (FXT) program. We report transverse mass spectra of protons, K^0_S and Λ, rapidity density distributions of $\pi^{\pm}$, K^0_S and Λ, directed flow of protons, $\pi^{\pm}$, K^0_S and Λ, and elliptic flow of protons and $\pi^{\pm}$. These are the first measurements of pion directed and elliptic flow in this energy region. Pion and proton elliptic flow show mass ordering. Measurements are compared with published results from AGS and RHIC. These results demonstrate that the STAR detector performs well in the FXT configuration.

Keywords: STAR, fixed-target, FXT, spectra, directed flow, elliptic flow, strangeness, rapidity density

1. Introduction

The goals of the STAR beam energy scan (BES) program include searches for a possible QCD critical point, and for the turn-off of signatures of quark-gluon plasma (QGP); study of the transition between hadronic and partonic matter is also of great interest [1]. RHIC BES phase I (BES-I) has yielded interesting results below $\sqrt{s_{NN}}$ = 19.6 GeV in azimuthal anisotropy for identified hadrons, kaon to pion ratios, and net-proton higher moments. These features continue to the lowest RHIC collider-mode energy, $\sqrt{s_{NN}}$ = 7.7 GeV, and motivate investigation at even lower energies. The STAR fixed-target (FXT) program [2] extends the energy reach from $\sqrt{s_{NN}}$ = 7.7 GeV to $\sqrt{s_{NN}}$

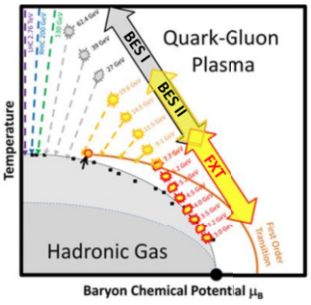

Fig. 1: Schematic QCD phase diagram, illustrating the conjectured critical point, phase transition lines, and the range of the FXT program and beam energy scan in collider mode.

[1] A list of members of the STAR collaboration and acknowledgements can be found at the end of this issue.

https://doi.org/10.1016/j.nuclphysa.2018.10.051

= 3.0 GeV, corresponding to baryon chemical potentials from 420 MeV to about 720 MeV. The directed flow (v_1) for protons and Λ hyperons at 7.7 GeV and above [3, 4] suggests a qualitative resemblance to the "softest point" of the equation of state predicted by hydrodynamic models.

Net-proton higher moment measurements from energies below 7.7 GeV could help determine the type of phase transition or reveal evidence for critical fluctuations [5]. However, RHIC cannot operate in collider mode below 7 GeV, due to steeply decreasing luminosity. By inserting a target into the beam pipe and circulating one beam in RHIC, we can study FXT collisions below $\sqrt{s_{NN}}$ = 7 GeV. Figure 1 shows an example of a schematic phase diagram, and illustrates the possible region probed by FXT measurements.

During a brief test in 2015, STAR collected approximately 1.3 million FXT events with centrality 0-30%.

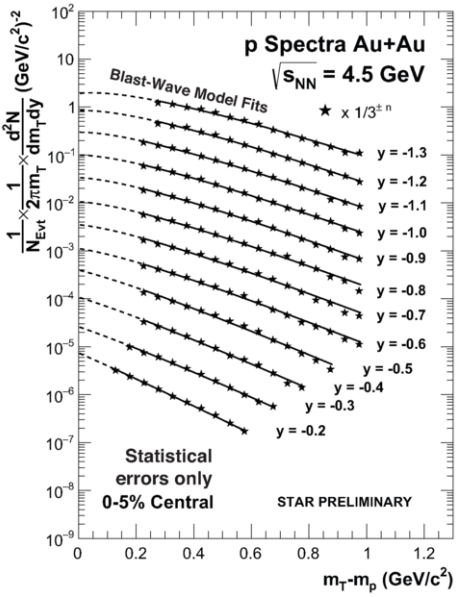

Fig. 2: Proton transverse mass spectra in 4.5 GeV Au+Au collisions.

2. Results

2.1. STAR FXT Particle Yield Results

Figure 2 presents proton spectra for 0-5% centrality in Au+Au collisions at $\sqrt{s_{NN}}$ = 4.5 GeV as a function of transverse mass $m_T - m_p$ in several rapidity bins, each with a width $\Delta y = 0.1$. These spectra were fitted using the Blast-Wave model, after correcting for detector efficiency, acceptance, energy loss and hadronic background. Overall, fits describe the data across the STAR FXT acceptance range.

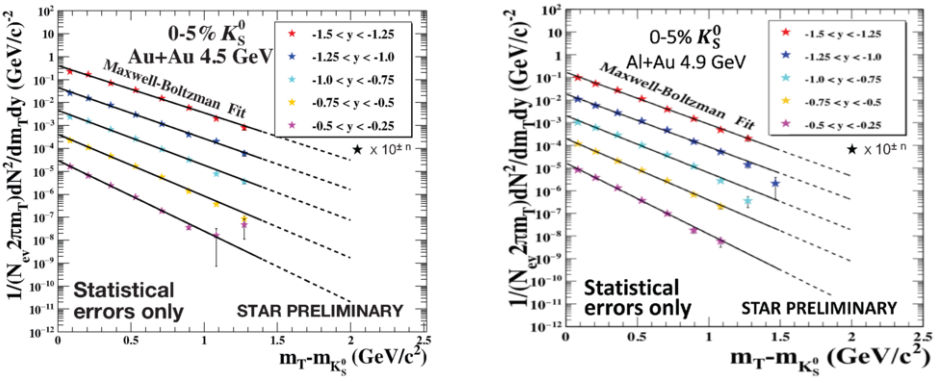

Fig. 3: K^0_S transverse mass spectra for central $\sqrt{s_{NN}}$ = 4.5 GeV Au+Au and 4.9 GeV Al+Au collisions.

In Fig. 3, m_T spectra of K^0_S from 4.5 GeV Au+Au and 4.9 GeV Al+Au collisions are shown for 0-5% centrality in several rapidity bins of width $\Delta y = 0.25$. These spectra are fitted using a Maxwell-Boltzmann functional form. The spectra and fits for Λ (not shown) are found to be similar to Fig. 3 in their range and fit quality. Kaon rapidity densities, dN/dy, are extracted from the fits and compared with AGS results in Fig. 4 (left). The STAR K^0_S dN/dy falls between E917 K^+ and K^- results and are slightly lower than $(K^+ + K^-)/2$ from E917 [6]. The amplitudes and widths of the current K^0_S dN/dy indicate good agreement between STAR FXT and published AGS results.

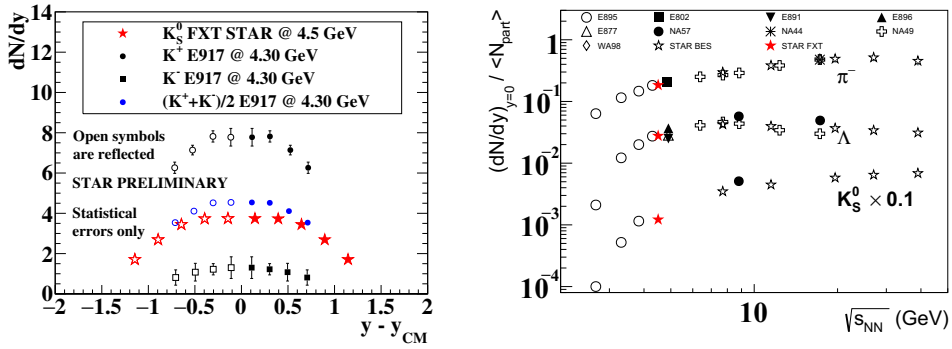

Fig. 4: (Left) Kaon dN/dy for Au+Au at or near 4.5 GeV. (Right) Peak dN/dy vs. beam energy for π^-, Λ and K^0_S.

In Fig. 4 (right), dN/dy distributions of π^-, K^0_S and Λ obtained in Au+Au collisions at $\sqrt{s_{NN}} = 4.5$ GeV near mid-rapidity, normalized by mean participant number $N_{\rm part}$, are compared across various experiments as a function of beam energy. The current STAR FXT rapidity densities are consistent with the trends defined by prior measurements at higher and lower energies [7–16].

2.2. STAR FXT Flow Results

The left panel of Fig. 5 presents proton $v_1(y)$ from 4.5 GeV Au+Au (red markers). E895 data for 4.3 GeV Au+Au at similar p_T and centrality are also plotted [17]. STAR FXT results are consistent with E895 but have much smaller statistical errors. In the right panel of Fig. 5, proton $v_1(y)$ is plotted in narrow intervals of p_T. The proton acceptance in FXT mode at this beam energy, with the standard selection of $0.4 < p_T < 2.0$ GeV/c used in prior studies [3, 4, 17], was found to have negligible impact on proton $v_1(y)$ down to $y - y_{cm} = 0$.

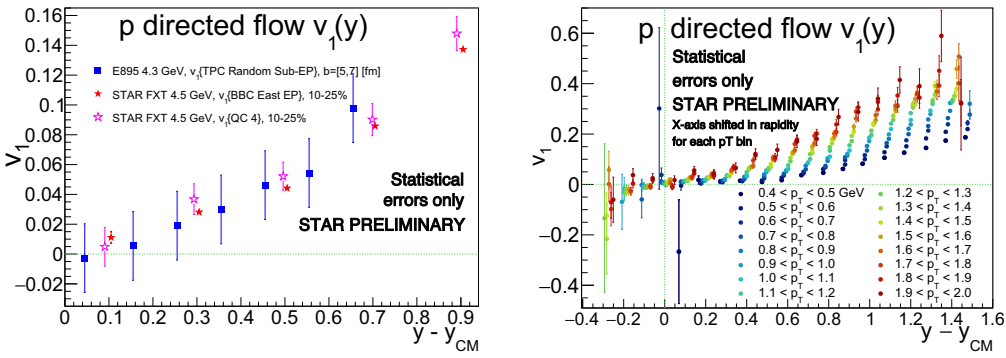

Fig. 5: (Left) proton $v_1(y)$ for FXT 4.5 GeV Au+Au, based on two separate methods [18, 19], and compared with E895 [17]. (Right) The same FXT proton $v_1(y)$ in narrow intervals of transverse momentum.

FXT directed flow slope dv_1/dy near midrapidity for protons, $\pi^{\pm}$, K^0_S and Λ at 4.5 GeV are compared in the left panel of Fig. 6 with STAR collider-mode results [3, 4] and with E895 [17]. The STAR FXT $\pi^{\pm}$ and K^0_S measurements continue the trend of negative dv_1/dy for mesons observed at 7.7 GeV and above. The STAR FXT dv_1/dy for protons at 4.5 GeV is in good agreement with E895 at 4.3 GeV, and both are consistent with a smooth interpolation between higher and lower energies.

Figure 7 presents FXT 4.5 GeV Au+Au proton and pion elliptic flow $v_2(p_T)$. The observed mass ordering of proton and pion v_2 resembles measurements at higher energies [20–22].

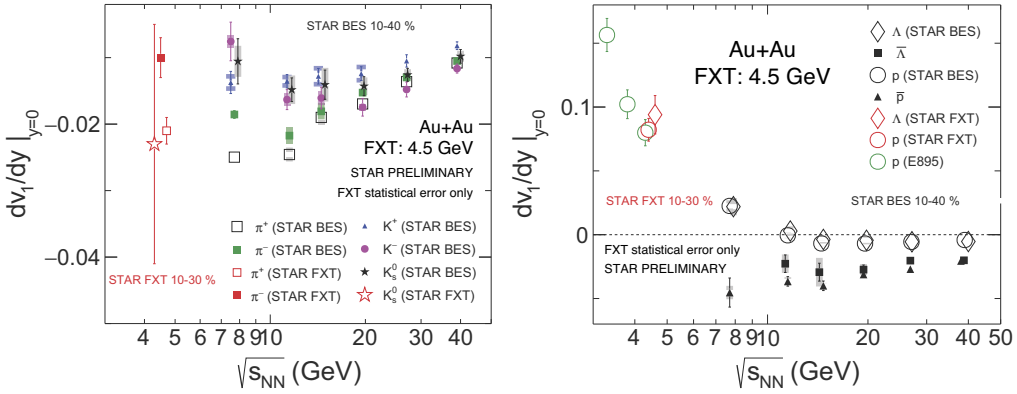

Fig. 6: Mid-rapidity directed flow slope versus beam energy for mesons (left panel) and for baryons (right panel).

3. Future FXT Plans

In future runs, STAR will have multiple detector upgrades [23], including the Inner Time Projection Chamber (iTPC), Endcap Time Of Flight (eTOF) and Event Plane Detector (EPD). The EPD is already in operation. These upgrades extend the detector acceptance, and improve the particle identification capability, event plane resolution and centrality determination. Running in FXT mode for two days at each of several energies between $\sqrt{s_{NN}}$ = 3.0 GeV and 7.7 GeV will permit acquisition of ~100 million events per energy and will extend the reach of baryon chemical potential to about 720 MeV. The highest FXT energy will overlap with the lowest collider-mode energy, allowing detailed cross checks.

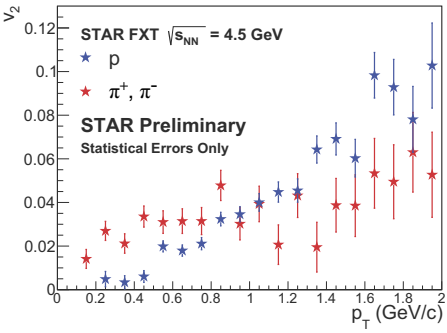

Fig. 7: 4.5 GeV Au+Au $v_2(p_T)$ for $\pi^{\pm}$ and protons.

References

[1] M. M. Aggarwal, *et al.*, arXiv:1007.2613.
[2] K. Meehan, for the STAR collaboration, Nucl. Phys. A **967** (2017) 808.
[3] L. Adamczyk, *et al.*, (STAR Collaboration), Phys. Rev. Lett. **112** (2014) 162301.
[4] L. Adamczyk, *et al.*, (STAR Collaboration), Phys. Rev. Lett. **120** (2018) 062301.
[5] X. Luo, N. Xu, Nucl. Sci. Tech. 28 (2017) 112.
[6] C. A. Ogilvie, (E802, E917 collaboration), Nucl. Phys. A **630** (1998) 571C.
[7] S. Albergo, *et al.*, Phys. Rev. Lett. **88** (2002) 062301.
[8] I. G. Bearden, *et al.*, (NA44 Collaboration), Phys. Rev. C **66** (2002) 044907.
[9] M. Gazdzicki, for the NA49 Collaboration, J. Phys. G: NPP **30** (2004) S701.
[10] T. Anticic, *et al.*, (NA49 Collaboration), Phys. Rev. Lett. **93** (2004) 022302.
[11] M. M. Aggarwal, *et al.*, (WA98 Collaboration), Phys. Rev. C **67** (2003) 014906.
[12] J. L. Klay, *et al.*, (E895 Collaboration), Phys. Rev. Lett. **88** (2002) 102301; Phys. Rev. C **68** (2003) 054905.
[13] C. Pinkenburg, for the E895 collaboration, Nucl. Phys. A **698** (2002) 495.
[14] Y. Akiba, *et al.*, Nucl. Phys. A **610** (1996) 139.
[15] J. Barrette, *et al.*, (E877 Collaboration), Phys. Rev. C **63** (2000) 014902.
[16] S. Ahmad, *et al.*, Phys. Lett. B **382** (1996) 35.
[17] H. Liu, *et al.*, (E895 Collaboration), Phys. Rev. Lett. **84** (2000) 5488.
[18] A. M. Poskanzer, S. A. Voloshin, Phys. Rev. C **58** (1998) 1671.
[19] A. Bilandzic, R. Snellings, S. Voloshin, Phys. Rev. C **83** (2011) 044913.
[20] J. Adams, *et al.*, (STAR Collaboration), Nucl. Phys. A **757** (2005) 102.
[21] L. Adamczyk, *et al.*, (STAR Collaboration), Phys. Rev. C **88** (2013) 014902.
[22] L. Adamczyk, *et al.*, (STAR Collaboration), Phys. Rev. C **93** (2016) 014907.
[23] Q. Yang, for the STAR collaboration, Proceedings Quark Matter 2018.